



Control of an Energy Efficient Hydraulic Cylinder Drive with Multiple Pressure Lines

N. H. Pedersen, S. Jensen, R. Hansen, A. Hansen, T. O. Andersen

Fluid Power and Mechatronic Systems, Department of Energy Technology, Aalborg University, Pontoppidanstraede 111, 9220 Aalborg, Denmark. E-mail: nhp@et.aau.dk, soerenchristianjensen@gmail.com, rhh@rdas.dk, ahh@et.aau.dk, toa@et.aau.dk

Abstract

This paper concerns a novel energy efficient hydraulic cylinder drive concept, consisting of three pressure lines used to supply a hydraulic cylinder(s). The proposed concept allows for reduced throttling losses compared to conventional solutions, while maintaining accurately cylinder control. One application where the concept shows great potential is as the actuation system for life tests of large mechanical structures, where structure deflections is made through cylinder force control. This work contributes to the development and control of this hydraulic concept, where the purpose is to obtain a high energy efficiency and an accurate cylinder force control. The final concept design is implemented in simulation models, where the performance of the developed control system is investigated to verify that the control performance is satisfactory. Furthermore, the energy efficiency is compared to a conventional hydraulic concept to verify the feasibility. Through simulation models, control performance similar to a conventional hydraulic concept has been obtained with the proposed control structure, while reducing the hydraulic energy consumption by up to 50%. Based on the findings in this paper it is assessed that the concept is ready for experimental validation.

Keywords: Hydraulics, Fluid Power, Energy efficient, Multiple Pressure Lines, Mechanical Life Tests

1 Introduction

When performing accelerated life tests of large mechanical structures, hydraulic cylinders are often used as actuation due to their high power density. In these tests, cyclic loads are often applied for long time periods where a perfect system up-time is preferable, such that the hydraulic system must provide great redundancy. Often, several cylinders are used simultaneously to cause the desired structure deflection, where each of these cylinders may have very different loads. Since the power used to deflect these large structures is high, the accumulated energy consumption may become tremendous. As a result, there is a desire of developing new alternative hydraulic concepts with a high energy efficiency. Since it is very important that the applied loads to the mechanical structure is accurately controlled for

such tests, the new concepts must maintain great control accuracy.

Various energy efficient hydraulic actuation systems have been studied both in academia and industry. Direct cylinder drives based on variable displacement units, rectifying bridges, hydraulic accumulator and/or other energy recovering solutions have been proposed (Heybroek et al., 2008, 2006; Ivantysynova and Rahmfeld, 1998; Zimmerman and Ivantysynova, 2011; Mingdong and Dingxuan, 2011). Alternatively, low cost solution direct pump control concept has been investigated (Schmidt et al., 2017, 2015; Ketelsen et al., 2018). However, all of these concepts require multiple pump units for each cylinder to achieve the desired redundancy, why the solutions become both expensive and complex. Recently emerging technologies,

feature digital hydraulics and hydraulic transformers. The hydraulic transformer is an energy efficient solution for converting hydraulic fluid pressure levels for multiple-cylinders (Inderelst et al., 2010; Shen et al., 2013; Guanzhong and Jihai, 2015). Digital hydraulics is another alternative and highly energy efficient solution allowing for direct cylinder control (Heikkila and Linjama, 2013; Heikkila et al., 2010; Linjama and Huh-tala, 2010; Ehsan et al., 1997; Payne et al., 2005). However, no commercial available solutions based on these technologies exist. An alternative solution is to use an additional pressure-line with a pressure level located in between the pump and tank pressure. This provides the potential of reducing the throttling losses at lighter loads and enables multiple cylinders to be connected to each pressure line. Digital valves have previously been used to switch between active pressure lines efficiently, but this induces severe pressure pulsations (Hansen et al., 2013) and does not allow for accurate cylinder control. To obtain continuous cylinder control (Dengler et al., 2012), (Dengler and von Dombrowski, 2012), and (Dengler et al., 2011) introduced a 4/3 spool-valve placed between the on/off valves and each cylinder. In this paper, a novel energy efficient hydraulic concept with the capability of recovering potential energy, while reducing energy losses due to throttling is proposed. This concept will be referred to as the Multiple Pressure Line (MPL) concept, which is similar to the other multiple pressure line concepts. However, this concept uses high-bandwidth 2/2 proportional valves, which allows for accurate cylinder control without pressure pulsation due to digital valves. Since accurate cylinder force control is very important when performing life test of large mechanical structures, this paper mainly focuses on control development without fluctuation due to switching between pressure lines.

2 Hydraulic concept

The working principle of the MPL concept in this study is described based on the schematic shown in Fig. 1. The spring load is used to emulate the stiffness of the mechanical structure. The MPL concept consist of three pressure lines with different pressure levels used to supply the cylinder. The three pressure lines may be categorized as a high, an intermediate and a low pressure line.

- **High pressure line (red):** Primary energy supply line pressurized at up to 350 bar by hydraulic pumps.
- **Intermediate pressure line (green):** Allows

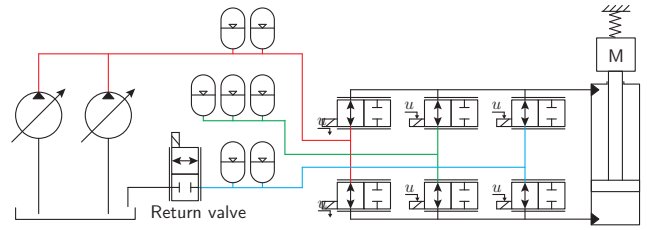


Figure 1: MPL concept capable of recovering potential energy and reducing throttling losses.

for recovery of hydraulic energy and reduced throttling losses.

- **Low pressure line (blue):** Pressurized return line at approximately 20 bar.

It may be seen that the hydraulic cylinder is operated by six 2/2-way proportional valves connecting the three pressure lines to both cylinder chambers. The concept allows for additional multiple parallel connected cylinders as an energy efficient alternative to e.g. load sensing solutions. The cylinder is operated by controlling the spool position of the proportional valves based on supplied voltage inputs. During normal operation, a single valve is active on both the rod and piston side of the cylinder. One pressure line is hence used to supply the cylinder with a flow, while the other is receiving the return flow. Using three pressure lines yields nine possible combinations of connecting the pressure lines to the piston and rod side. The combinations yield a maximum possible cylinder force, called force states, each having a maximum available force, F_{avail} , which may be determined by (1), when neglecting losses.

$$F_{\text{avail}} = A_p p_p - A_r p_r \quad (1)$$

A_p and A_r are the cylinder areas, while p_p and p_r are the chamber pressures for the piston and rod side respectively. An illustration of the magnitude of the nine force states are shown in Fig. 2 based on pressure line levels of 350, 185, and 20bar. The abbreviations LP, IP and HP refer to the low, intermediate and high pressure line. As an example, the highest positive available force is obtained by connecting the high pressure line to the piston side and the low pressure line to the rod side, illustrated as force state $\mathcal{F} = 9$.

With the MPL concept, the throttling losses may be reduced by switching between force states depending on the required actuation force. How the throttling losses are reduced by switching between force states compared to a conventional 4/3-way spool valve system with a constant supply pressure is illustrated in Fig. 3 for an arbitrary constructed load cycle.

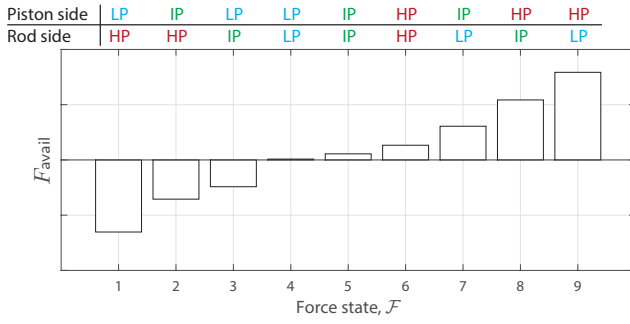


Figure 2: Available cylinder forces depending on the pressure line combinations.

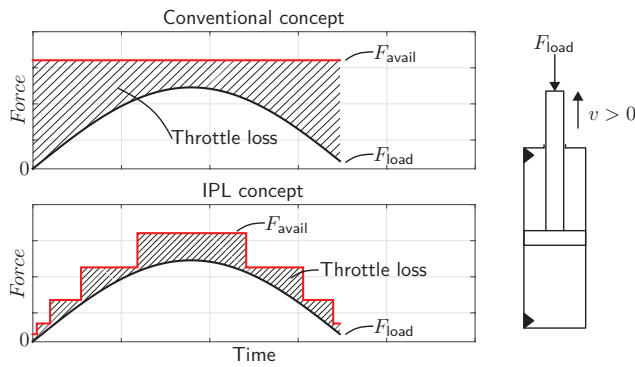


Figure 3: Comparison of a conventional concept and the IPL concept, for an arbitrary operation cycle.

It may be observed that the available force, F_{avail} , always has to be greater than the required cylinder force, F_{load} , since the piston velocity, v , is positive. The difference between the available force and the load force may be seen as losses (Hatched area) that are throttled away in the form of a pressure drop across the valves.

2.1 Potential Energy Recovery

The potential energy released from the mechanical structure (simplified to be a spring) may be recovered and stored as hydraulic energy in the accumulators connected to the pressure lines. The accumulators are charged when the return side of the cylinder is connected to the associated pressure line. Likewise, the accumulators are discharged when the associated pressure line is connected to the supply side of the cylinder. How the accumulators are used for supplying and recovering energy in the system is illustrated in Fig. 4 based on a simplified operation scenario against a spring load.

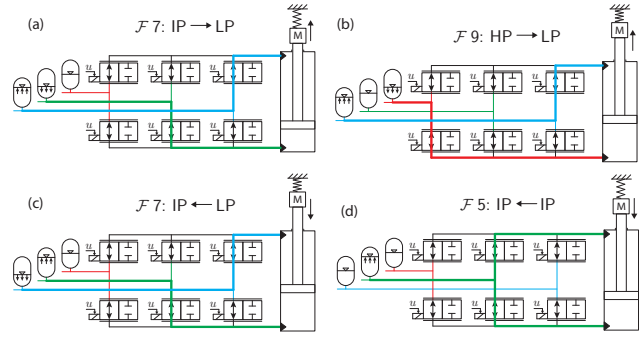


Figure 4: Simplified operation scenarios against a spring load.

Initially the cylinder is extended against the spring illustrated in (a). This is done using force state 7, where the accumulator in the intermediate pressure line is discharged by supplying flow to the cylinder piston side, while the accumulator in the low pressure line is charged by the return flow. As the spring is compressed, a higher force is required to compress it. This is illustrated in (b), where the larger force state 9 is used. Here the cylinder is supplied by the high pressure line, while the accumulator in the low pressure line is further charged by the return flow. When retracting the cylinder, force state 7 may be used as shown in (c). Since the magnitude of the spring load is larger than the used force state, the flow is reversed compared to (a), such that the accumulator in the intermediate pressure line is charged, while the low pressure line is used as the supply. During retraction of the cylinder the spring load decreases and as a result a lower force state is used. This is seen in (d), where the intermediate pressure line is used for both supplying and receiving flow to and from the cylinder. As a result, the accumulator in the intermediate pressure line is charged by a net positive flow into the line.

It is evident that the MPL concept has a reduced energy consumption compared to a conventional hydraulic system using a 4/3-way spool valve and a constant supply pressure. However, several complications must be solved for the concept to be a feasible solution. An accurate control of the cylinder force is required to obtain precise control of the loads applied to the mechanical structure. Therefore, switchings between the pressure lines should be conducted such that these do not influence the accuracy of the cylinder force control. Furthermore, since there is no external connections to the intermediate pressure line, the net flow in and out of the pressure line must be balanced over time to maintain an approximately constant pressure level. To achieve this, a hydraulic control system for the MPL concept has to be designed, which is the main focus of this paper

3 System Modeling

A non-linear dynamic model is set up for the system and is used as the basis for controller development and performance evaluation test of the MPL concept. All dimensions and parameter values used for modeling of the system may be found in Tab. 1. The mathematical model establishment is based on the illustration shown in Fig. 5.

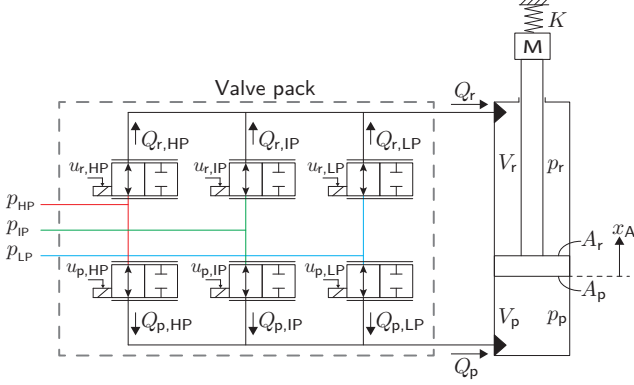


Figure 5: Illustration of a cylinder and the associated valve pack with defined variables used for modeling.

The dynamics of the cylinder piston movement is obtained by applying Newtons 2nd law of motion resulting in

$$M \ddot{x}_A = \underbrace{p_p A_p - p_r A_r}_{F_p} - K x_A - F_{\text{fric}} \quad (2)$$

where M is the equivalent mass moment of inertia of the cylinder and mechanical structure and K is the equivalent spring constant of the mechanical structure. The cylinder friction force, F_{fric} , is modeled by a viscous, a Coulomb and a Stribeck term, where a hyperbolic tangent function is used to avoid numerical simulation problems near the vicinity of zero velocity. The friction model is given as

$$F_{\text{fric}} = \underbrace{B_c \dot{x}_A}_{\text{Viscous}} + \tanh \frac{1.25}{v_{\text{br}}} \dot{x}_A \left(\underbrace{(F_c + k_{\text{Cp}} (p_p - p_r))}_{\text{Coulomb}} + \underbrace{\left(1 + (aBr - 1) 2.1 e^{\left(\frac{-|\dot{x}_A|}{v_{\text{br}}} \right)} \right)}_{\text{Stribeck}} \right) \quad (3)$$

B_c is the viscous friction coefficient, F_c is the static Coulomb friction coefficient and k_{Cp} is a coefficient describing the Coulomb friction due to the cylinder chambers pressure difference. v_{br} denotes the break away velocity, where the maximum friction force occurs and aBr is the factor between the break away friction force and the nominal Coulomb friction force. The friction force as function of piston velocity is shown in Fig. 6a at nominal pressure difference.

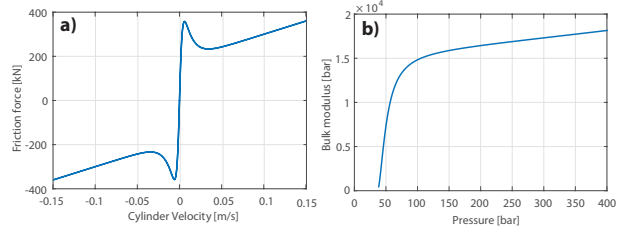


Figure 6: a) Friction force as a function of cylinder velocity with $\Delta p = 220$ bar. b) Effective bulk modulus as function of pressure.

The pressure build up in the cylinder chambers is described by the continuity equation to be those given by

$$\begin{aligned} \dot{p}_p &= (Q_p - A_p \dot{x}_A) \frac{\beta_e(p_p)}{V_{p,\text{init}} + A_p x_A} \\ \dot{p}_r &= (Q_r + A_r \dot{x}_A) \frac{\beta_e(p_r)}{V_{r,\text{init}} - A_r x_A} \end{aligned} \quad (4)$$

$V_{p,\text{init}}$ and $V_{r,\text{init}}$ are the initial chamber volumes of the piston and rod side respectively. The effective bulk modulus, β_e , is modeled pressure dependent as is shown in Fig. 6b.

The piston and rod side flows to the cylinder may be described by the sum of flows through the valves on the respective side as seen in Fig. 5. The flows Q_p and Q_r may hence be described by

$$\begin{aligned} Q_p &= Q_{p,\text{HP}} + Q_{p,\text{IP}} + Q_{p,\text{LP}} \\ Q_r &= Q_{r,\text{HP}} + Q_{r,\text{IP}} + Q_{r,\text{LP}} \end{aligned} \quad (5)$$

Each of the flows through the valves is modeled by a modified orifice equation based on information specified in the data-sheet of the valve. The flows through the valves are given by

$$\begin{aligned} Q_{p,\text{line}} &= Q_n A_v(x_{vp,\text{line}}) \sqrt{\frac{|p_{\text{line}} - p_p|}{\Delta p_n}} \text{sign}(p_{\text{line}} - p_p) \\ Q_{r,\text{line}} &= Q_n A_v(x_{vr,\text{line}}) \sqrt{\frac{|p_{\text{line}} - p_r|}{\Delta p_n}} \text{sign}(p_{\text{line}} - p_r) \end{aligned} \quad (6)$$

for line = [HP IP LP]

Q_n and Δp_n are the nominal flow through the valve and pressure drop across the valve. The normalized valve opening area A_v is modeled as a function of the spool position x_v in accordance with the data-sheet. The dynamics of the valve (Parker NG25 (Parker, 2015)) spool position is modeled as a second order system with a slew rate limiter. The dynamics are described by (7), where ω_v and ζ_v are the eigen-frequency and damping

coefficient respectively.

$$\begin{aligned} \frac{x_{vp,line}}{u_{p,line}} &= \frac{\omega_v^2}{s^2 + 2\zeta_v \omega_v s + \omega_v^2} \quad \text{for line} = [\text{HP IP LP}] \\ \frac{x_{vr,line}}{u_{r,line}} &= \frac{\omega_v^2}{s^2 + 2\zeta_v \omega_v s + \omega_v^2} \quad \text{for line} = [\text{HP IP LP}] \end{aligned} \quad (7)$$

The voltage input, u , valve position, x_v , as well as the opening area, A_v , are normalized to be between zero and one. The maximum opening area of one is hence obtained with a spool position of one, when the applied voltage input is one. This way the nominal flow through the valve is obtained with a unity voltage input and a nominal pressure difference across the valve. The same valve model is used for the larger return valve (Parker NG40 (Parker, 2015)) used to control the return flow to the tank.

The variables used to derive the model for the pressure line dynamics is shown in Fig. 7.

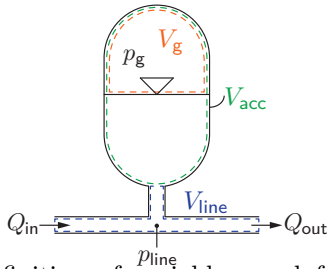


Figure 7: Definition of variables used for the simple pressure line model.

Q_{in} and Q_{out} are the flows entering and leaving the pressure line. V_g is the volume of the gas, p_g is the gas pressure, p_{line} is the line pressure, V_{acc} is the total accumulator volume, and V_{line} is the pressure line volume. p_{line} hence denotes either p_{HP} , p_{IP} , or p_{LP} , depending on the pressure line being modeled. The pressure in one of the pressure lines is described by the continuity equation to the left hand side in (8), while the change in gas volume is described by the right hand side equation.

$$\dot{p}_{line} = \left(Q_{in} - Q_{out} + \dot{V}_g \right) \frac{\beta_e(p_{line})}{V_{tot}} \quad \dot{V}_g = \frac{-1}{\kappa} \frac{V_g}{p_g} \dot{p}_g \quad (8)$$

The polytropic gas constant κ is chosen to yield an adiabatic process where losses due to heat dissipation is neglected. V_{tot} is the total oil volume in the line and accumulator calculated as $V_{tot} = V_{line} + V_{acc} - V_g$.

Since the volume of the gas V_g cannot exceed the total accumulator volume V_{acc} , the gas volume is mod-

eled as follows

$$V_g = \begin{cases} V_{acc} & \text{if } p_{line} < p_{g0} \\ V_{acc} \left(\frac{p_{g0}}{p_{line}} \right)^{\frac{1}{\kappa}} & \text{otherwise} \end{cases} \quad (9)$$

p_{g0} is the pre-charge pressure of the gas in the accumulator. By neglecting the mass and friction of the moving barrier between gas and fluid in the accumulator, the pressure of the gas and oil may be considered equal: $p_g = p_{line}$. By combining the two equations in (8) and inserting this relationship, the final pressure line model is obtained to be that given by

$$\dot{p}_{line} = (Q_{in} - Q_{out}) \frac{1}{\frac{V_{tot}}{\beta_e(p_{line})} + \frac{1}{\kappa} \frac{V_g}{p_{line}}} \quad (10)$$

The pressure line model in (10) is applied on the three pressure lines. The pressure line flows in and out of the lines, Q_{in} and Q_{out} are determined by (11), based on a combination of the hydraulic schematics shown in Fig. 1 and Fig. 5.

$$\begin{aligned} Q_{in,HP} - Q_{out,HP} &= Q_{pump} - \underbrace{(Q_{p,HP} + Q_{r,HP})}_{Q_{HP}} \\ Q_{in,IP} - Q_{out,IP} &= - \underbrace{(Q_{p,IP} + Q_{r,IP})}_{Q_{IP}} \\ Q_{in,LP} - Q_{out,LP} &= - \underbrace{(Q_{p,LP} + Q_{r,LP})}_{Q_{LP}} - Q_{return} \end{aligned} \quad (11)$$

Q_{HP} , Q_{IP} and Q_{LP} is hence the sum of the flows from the high, intermediate and low pressure line respectively. Q_{return} is the flow through the return valve in the low pressure line.

The dynamics of the pumps are modeled as a second order system with a slew rate limiter. The pumps are controlled by a control signal, u_{pump} , which is normalized to have a value between zero and one. The pump model is given as

$$\frac{Q_{pump}}{u_{pump}} = K_{pump} \frac{\omega_p^2}{s^2 + 2\zeta_p \omega_p s + \omega_p^2} \quad (12)$$

Q_{pump} is the pump flow and K_{pump} is the flow gain which determines the pump size. ω_p is the small signal bandwidth, and ζ_p is the damping coefficient.

4 Hydraulic Control System

When developing the control strategy for the system it is initially considered that only the low and high pressure lines are active, similar to a separate metering system. The cylinder force control structure for the system hence reduces to that shown in Fig. 8, for the simplified model with two pressure lines.

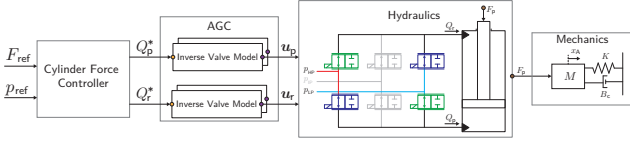


Figure 8: Schematic of the simplified hydraulic system to be controlled.

With two inputs it is possible to control two outputs, why it is chosen to also control one of the cylinder pressures similar to a conventional separate metering concept. For positive piston movement, the blue valves are activated, while the green valves are activated for movement in the opposite direction. The control strategy is based around being able to obtain the desired flow on the piston and rod side, yielding the desired pressures and thus resulting in the force being equal to its reference. To obtain the desired flows, an inverse model strategy called active gain compensation (AGC) is used to convert flow references to valve inputs based on the measured pressure drop across the valves as shown in Fig. 9.

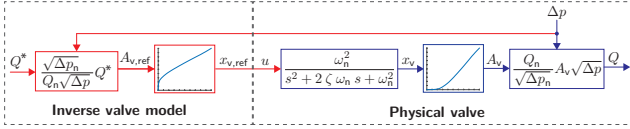


Figure 9: Active gain compensation structure used to obtain the valve voltage input.

The flow references Q_p^* and Q_r^* are given to both valves on the piston and rod side respectively. However, the AGC is implemented such that only a single valve is active at any time on the piston and rod side. This is done by use of the inverse valve model given as

$$A_{v,ref} = \begin{cases} \frac{\sqrt{\Delta p_n}}{Q_n \sqrt{\Delta p}} Q^* & \text{if } \text{sign}(Q^*) = \text{sign}(\Delta p) \\ 0 & \text{otherwise} \end{cases} \quad (13)$$

where Δp is the measured pressure drop across the specific valve. The valve opening area reference is used in a lookup table, which has the valve position reference $x_{v,ref}$ as output. This output is limited to one, why an opening area value of one or above results in a fully open valve. For the valves connected to the high pressure line, the value of Δp is always positive. Therefore, these valves are only active when the flow reference, Q^* , is positive, since Q_n and Δp_n are positive constants. Likewise, for the valves connected to the low pressure line, the value of Δp is always negative. These valves are hence only active when a negative flow reference, Q^* , is given.

4.1 Linear model development

A linear representation of the model is set up and used for system analysis and controller development. In the linear model it is assumed that only a single 2/2-way valve is active at any time on both the piston and rod side, which is valid in the above case with two pressure lines. A linear representation of the mechanical system is obtained by omitting the static friction force yielding

$$M \ddot{x}_A = p_p A_p - p_r A_r - K x_A - B_c \dot{x}_A \quad (14)$$

The continuity equations describing the pressure build up in the cylinder chambers are linearized by assuming constant chamber volumes and effective bulk modulus. A linear representation of the continuity equations hence become those derived to be

$$\dot{p}_p = (Q_p - A_p \dot{x}_A) \frac{\beta_{p,0}}{V_{p,0}} \quad \dot{p}_r = (Q_r + A_r \dot{x}_A) \frac{\beta_{r,0}}{V_{r,0}} \quad (15)$$

Variables denoted by 0 indicate the value after inserting the linearization point. For linearization of the orifice equation, describing the flows to the cylinder, the following assumptions have been made: The valve opening area with respect to the spool position is linear between closed and fully opened. The flow into the piston side chamber is positive and the flow into the rod side chamber is negative (corresponding to positive piston movement). Additionally, the pressure in the pressure lines is considered constant. Based on these simplifications, the orifice equations may be reduced to those given by

$$Q_p = \underbrace{\frac{Q_n}{\sqrt{\Delta p_n}}}_{k_q} x_{vp} \sqrt{p_{HP} - p_p} \quad (16)$$

$$Q_r = - \underbrace{\frac{Q_n}{\sqrt{\Delta p_n}}}_{k_q} x_{vr} \sqrt{p_r - p_{LP}}$$

By application of a first order Taylor approximation the linear models of the flow equations become

$$\delta Q_p = \underbrace{k_q \sqrt{p_{HP,0} - p_{p,0}}}_{K_{qpx}} \delta x_{vp} - \underbrace{\frac{k_q x_{vp,0}}{2 \sqrt{p_{HP,0} - p_{p,0}}}}_{K_{qpp}} \delta p_p$$

$$\delta Q_r = - \underbrace{k_q \sqrt{p_{r,0} - p_{r,0}}}_{K_{qrx}} \delta x_{vr} - \underbrace{\frac{k_q x_{vr,0}}{2 \sqrt{p_{r,0} - p_{r,0}}}}_{K_{qrp}} \delta p_r \quad (17)$$

A linear representation of the utilized AGC is made by using the linear valve model and neglecting the valve dynamics, such that $x_{vp} = u_p$ and $x_{vr} = u_r$. The

resulting linearized input to the valves is derived to be those given as

$$\begin{aligned}\delta Q_p &= K_{qpx} \delta x_{vp} - K_{qpp} \delta p_p \quad \longrightarrow \quad \delta u_p = \frac{1}{K_{qpx}} \delta Q_p^* + \frac{K_{qpp}}{K_{qpx}} \delta p_p \\ \delta Q_r &= -K_{qrx} \delta x_{vr} - K_{qrp} \delta p_r \quad \longrightarrow \quad \delta u_r = -\frac{1}{K_{qrx}} \delta Q_r^* - \frac{K_{qrp}}{K_{qrx}} \delta p_r\end{aligned}\quad (18)$$

The left hand side equations are the linearized valve model and the right hand side equations are the linearized inverse valve models used in the AGC.

4.2 State Space representation

To aid in the controller development and system analysis, the linearized system is rewritten into state space form. The general state space representation is given by

$$\dot{\mathbf{x}} = \mathbf{A} \mathbf{x} + \mathbf{B} \mathbf{u} \quad \mathbf{y} = \mathbf{C} \mathbf{x} + \mathbf{D} \mathbf{u} \quad (19)$$

The states are chosen to be $\mathbf{x} = [p_p \ p_r \ \dot{x}_A \ x_A \ \dot{x}_{vp} \ x_{vp} \ \dot{x}_{vr} \ x_{vr}]^T$, the outputs to be $\mathbf{y} = [F_p \ p_r]^T$, while the inputs are $\mathbf{u} = [Q_p^* \ Q_r^*]^T$. The rod side pressure is chosen as the controlled pressure, since it provides a slightly less cross coupled control system.

The state space representation of the system hence becomes that given in (20). Since the bulk modulus is approximately constant at the operation pressures the following assumption is made: $\beta = \beta_{p,0} = \beta_{r,0}$. Additionally, for simplicity of writing $V_r = V_{r,0}$ and $V_p = V_{p,0}$ is used in the remainder of this paper.

$$\begin{aligned}\begin{bmatrix} -\frac{\beta}{V_p} K_{qpp} & 0 & -\frac{\beta}{V_p} A_p & 0 & 0 & \frac{\beta}{V_p} K_{qpx} & 0 & 0 \\ 0 & -\frac{\beta}{V_r} K_{qrp} & \frac{\beta}{V_r} A_r & 0 & 0 & 0 & 0 & -\frac{\beta}{V_r} K_{qrx} \\ \frac{A_p}{M} & -\frac{A_r}{M} & -\frac{B_c}{M} & -\frac{K}{M} & 0 & 0 & 0 & 0 \\ 0 & 0 & 1 & 0 & 0 & 0 & 0 & 0 \\ \frac{K_{qpp}}{K_{qpx}} \omega_v^2 & 0 & 0 & 0 & -2\zeta_v \omega_v & -\omega_v^2 & 0 & 0 \\ 0 & 0 & 0 & 0 & 1 & 0 & 0 & 0 \\ 0 & -\frac{K_{qrp}}{K_{qrx}} \omega_v^2 & 0 & 0 & 0 & 0 & -2\zeta_v \omega_v & -\omega_v^2 \\ 0 & 0 & 0 & 0 & 0 & 0 & 1 & 0 \end{bmatrix} \mathbf{x} + \begin{bmatrix} \frac{\beta}{V_p} & 0 \\ 0 & \frac{\beta}{V_r} \\ 0 & 0 \\ 0 & 0 \\ 0 & 0 \\ 0 & 0 \\ 0 & 0 \\ 0 & 0 \end{bmatrix} \mathbf{u} = \begin{bmatrix} p_p \\ p_r \\ \dot{x}_A \\ x_A \end{bmatrix} \\ \begin{bmatrix} 0 & 0 & 0 & 0 & \frac{\omega_v^2}{K_{qpx}} & 0 & 0 & 0 \\ 0 & 0 & 0 & 0 & 0 & -\frac{\omega_v^2}{K_{qrx}} & 0 & 0 \end{bmatrix}^T \mathbf{x} + \begin{bmatrix} A_p & -A_r & 0 & 0 & 0 & 0 & 0 & 0 \\ 0/1 & 1/0 & 0 & 0 & 0 & 0 & 0 & 0 \end{bmatrix} \mathbf{x} \end{aligned}\quad (20)$$

For state feedback it is beneficial if the valve positions and velocities may be neglected, such that these are not measured and used for control. In the ideal case $Q_p = Q_p^*$ and $Q_r = Q_r^*$. To investigate if it is possible to consider the AGC ideal when synthesizing controllers, a comparison of the ideal case and non-ideal case is made. The frequency response of the system with and without AGC and valve dynamics is shown in Fig. 10.

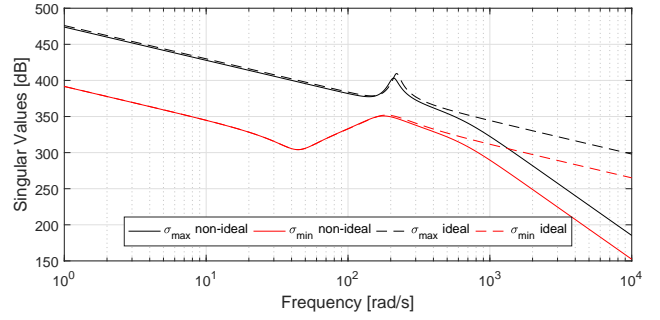


Figure 10: Singular values comparison between system with ideal and non-ideal valves.

It is seen that the frequency response may be considered identically up to the valves eigen-frequency of $\omega_v \approx 600$ rad/s. Therefore the phase may be considered identically up to a frequency of 60 rad/s. Since the control reference signals are cyclic with frequencies in the order of 1 rad/s, the controller is to be designed such that the closed-loop eigen-frequency is less than 60 rad/s. The valve dynamics is hence omitted in the following control design.

In the ideal case with the input being $\mathbf{u} = [Q_p \ Q_r]^T$, the state space representation of the system becomes that in (21) when truncating the full state model in (20). The state space model is obtained by use of (2) and (15).

$$\begin{aligned}\begin{bmatrix} \dot{p}_p \\ \dot{p}_r \\ \dot{x}_A \\ \dot{x}_A \end{bmatrix} &= \begin{bmatrix} 0 & 0 & -\frac{\beta}{V_p} A_p & 0 \\ 0 & 0 & \frac{\beta}{V_r} A_r & 0 \\ \frac{A_p}{M} & -\frac{A_r}{M} & -\frac{B_c}{M} & -\frac{K}{M} \\ 0 & 0 & 1 & 0 \end{bmatrix} \begin{bmatrix} p_p \\ p_r \\ \dot{x}_A \\ x_A \end{bmatrix} + \begin{bmatrix} \frac{\beta}{V_p} & 0 \\ 0 & \frac{\beta}{V_r} \\ 0 & 0 \\ 0 & 0 \end{bmatrix} \begin{bmatrix} Q_p \\ Q_r \end{bmatrix} \\ \begin{bmatrix} F_p \\ p_r \end{bmatrix} &= \begin{bmatrix} A_p & -A_r & 0 & 0 \\ 0 & 1 & 0 & 0 \end{bmatrix} \mathbf{x} \end{aligned}\quad (21)$$

The simplified system representation above is hence used for controller design.

4.3 Deterministic Optimal Control

A deterministic optimal control strategy in the form of a linear quadratic regulator (LQR) is used for control of the cylinder force. With the LQR method, a classical state feedback controller is designed by minimizing the cost function given by

$$\mathcal{J} = \int_0^\infty \mathbf{x}(t)^T \mathbf{Q} \mathbf{x}(t) + \mathbf{u}(t)^T \mathbf{R} \mathbf{u}(t) dt \quad (22)$$

where \mathbf{Q} and \mathbf{R} are weighting matrices for the states and inputs respectively. The importance of tracking each state to zero (or follow a reference in case of a servo problem) is hence specified in \mathbf{Q} and the importance of control effort to do so is specified in \mathbf{R} . The

designers choice hence lies in choosing the weighting matrices \mathbf{Q} and \mathbf{R} to obtain the desired closed loop properties.

Since it is desired to be able to specify the importance of the force tracking, a state transformation is made. The transformation is conducted by applying the state transformation matrix \mathbf{P} given by

$$\underbrace{\begin{bmatrix} F_p \\ p_r \\ \dot{x}_A \\ x_A \end{bmatrix}}_{\mathbf{z}} = \underbrace{\begin{bmatrix} A_p & -A_r & 0 & 0 \\ 0 & 1 & 0 & 0 \\ 0 & 0 & 1 & 0 \\ 0 & 0 & 0 & 1 \end{bmatrix}}_{\mathbf{P}} \underbrace{\begin{bmatrix} p_p \\ p_r \\ \dot{x}_A \\ x_A \end{bmatrix}}_{\mathbf{x}} \quad (23)$$

To ease the weighting significantly, the model with the new states \mathbf{z} , is normalized with respect to the expected maximum values. This follows that the references, inputs, states and outputs of the normalized plant, all have values between ± 1 . The scaling is performed by introducing the scaling matrices given by

$$\mathbf{D}_r = \begin{bmatrix} \hat{F}_p & 0 \\ 0 & \hat{p}_r \end{bmatrix} \mathbf{D}_u = \begin{bmatrix} \hat{Q}_p & 0 \\ 0 & \hat{Q}_r \end{bmatrix} \mathbf{D}_x = \begin{bmatrix} \hat{F}_p & 0 & 0 & 0 \\ 0 & \hat{p}_r & 0 & 0 \\ 0 & 0 & \hat{x}_A & 0 \\ 0 & 0 & 0 & \hat{x}_A \end{bmatrix} \quad (24)$$

The transformed and normalized state representation becomes that given by

$$\begin{aligned} \dot{\mathbf{z}}_n &= \underbrace{(\mathbf{D}_x^{-1} \mathbf{P}) \mathbf{A} (\mathbf{D}_x^{-1} \mathbf{P})^{-1}}_{\mathbf{A}_n} \mathbf{z}_n + \underbrace{(\mathbf{D}_x^{-1} \mathbf{P}) \mathbf{B} \mathbf{D}_u}_{\mathbf{B}_n} \mathbf{u}_n \\ \mathbf{y}_n &= \underbrace{\mathbf{D}_r^{-1} \mathbf{C} (\mathbf{D}_x^{-1} \mathbf{P})^{-1}}_{\mathbf{C}_n} \mathbf{z}_n \end{aligned} \quad (25)$$

The system is appended with an additional integral state vector given by (26) for disturbance rejection and to obtain unity dc-gain.

$$\dot{\mathbf{z}}_{\text{int}} = \mathbf{r}_n - \mathbf{y}_n = \mathbf{r}_n - \mathbf{C}_n \mathbf{z}_n \quad (26)$$

where \mathbf{r}_n is a vector containing the force and pressure reference. An integral state is hence added to both the force and pressure error. The new system with the appended integral states may be described by

$$\begin{aligned} \underbrace{\begin{bmatrix} \dot{\mathbf{z}}_n \\ \dot{\mathbf{z}}_{\text{int}} \end{bmatrix}}_{\dot{\mathbf{z}}_a} &= \underbrace{\begin{bmatrix} \mathbf{A}_n & \mathbf{0} \\ -\mathbf{C}_n & \mathbf{0} \end{bmatrix}}_{\mathbf{A}_a} \underbrace{\begin{bmatrix} \mathbf{z}_n \\ \mathbf{z}_{\text{int}} \end{bmatrix}}_{\mathbf{z}_a} + \underbrace{\begin{bmatrix} \mathbf{B}_n \\ \mathbf{0} \end{bmatrix}}_{\mathbf{B}_a} \mathbf{u}_n + \underbrace{\begin{bmatrix} \mathbf{0} \\ \mathbf{I} \end{bmatrix}}_{\mathbf{B}_r} \mathbf{r}_n \\ \mathbf{y}_n &= \underbrace{\begin{bmatrix} \mathbf{C}_n & \mathbf{0} \end{bmatrix}}_{\mathbf{C}_a} \mathbf{z}_a \end{aligned} \quad (27)$$

The optimal solution for the control law $\mathbf{u}_n = -\mathbf{K}_a \mathbf{z}_a$ may be derived to be that given by

$$\mathbf{0} = \mathbf{A}_a^T \mathbf{X} + \mathbf{X} \mathbf{A}_a - \mathbf{X} \mathbf{B}_a \mathbf{R}^{-1} \mathbf{B}_a^T \mathbf{X} + \mathbf{Q} \quad (28)$$

$$\mathbf{K}_a = \mathbf{R}^{-1} \mathbf{B}_a^T \mathbf{X} \quad (29)$$

By solving for the unique positive-semidefinite solution of \mathbf{X} in the algebraic Riccati equation in (28), the controller gains \mathbf{K}_a may be determined by (29). To improve the tracking performance further, flow feed-forward is implemented without destabilizing the system. The flow feed-forward is implemented on the form given by

$$\begin{bmatrix} Q_p^{**} \\ Q_r^{**} \end{bmatrix} = \begin{bmatrix} Q_p^* \\ Q_r^* \end{bmatrix} + K_{\text{ff}} \begin{bmatrix} A_p \\ A_r \end{bmatrix} \frac{1}{K_{\text{eq}}} \frac{d}{dt} F_{\text{ref}} \quad (30)$$

Q_p^{**} and Q_r^{**} are the new inputs with flow feed forward and Q_p^* and Q_r^* are the original inputs. The feed-forward is based on the assumption that the piston position is proportional to the force reference given by: $x_A \approx F_{\text{ref}}/K$, why the derivative of this yields the velocity. K_{ff} is the feed-forward coefficient, determining the amplitude of the feed-forward. In the presented results, the weighting matrices Q and R are chosen through a trial and error method, where the desire of achieving accurate tracking performance is weighted high resulting in

$$\mathbf{Q} = \mathbf{I}_{6 \times 6} [1 \ 1 \ 0.01 \ 0.01 \ 25e6 \ 2e6]^T \mathbf{R} = \begin{bmatrix} 1 & 0 \\ 0 & 1 \end{bmatrix}^T \quad (31)$$

4.4 Optimal Control Performance

Initially, the control performance of the designed controllers is investigated on the system, where only the high and low pressure lines are used. A simple proportional controller is used to maintain a stable supply and tank pressure, p_{HP} and p_{LP} respectively, that is within ± 5 bar of its constant reference value. Due to the simplicity of this controller, the design of it is not documented. The performance test is used to give an indication of the best possible tracking performance, since no switching between pressure lines is yet implemented. This system is equivalent to a conventional separate metering system and is in the remainder of the paper described as the conventional system. Simulation results for a load test of a large mechanical structure when using the designed controllers is seen in Fig. 11. Six cylinders connected to the common lines and with different load scenarios has been simulated to illustrate the performance in various cases. The pressure reference is shaped linearly to be in counter-phase with the force reference given by (42). It is chosen to only show the references and errors, since the responses would be identical to the references with the shown axis limits. It is seen that the maximum cylinder force error is $\approx \pm 10$ kN, which correspond to an error of $\approx 0.2\%$. Tiny fluctuations are observed in the errors when the piston direction of motion is changed and the active valves are switched. The fluctuations are induced due

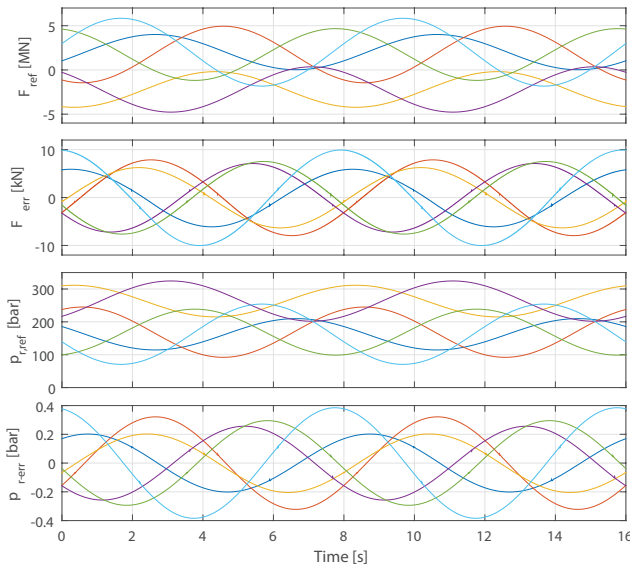


Figure 11: Simulated system response for cylinder force control using two pressure lines.

to the dead band in the valves and the sign change of the Coulomb friction. These fluctuations are however so small that they in general may be neglected. It is seen that the error in the pressures are very low and are at maximum $\approx \pm 0.4$ bar, which correspond to an error of $\approx 0.12\%$.

The results obtained in Fig. 11 are a best case scenario where the intermediate pressure line is not used, such that the active valves are only switched when the direction of piston motion is changed. The objective is hereafter to design the switching system, such that the control performance with three pressure lines is as similar as possible to that obtained for the best case scenario.

5 Pressure Line Switching System

The development of strategies for switching between pressure lines is based on the previously presented model, but contrary to earlier, the cylinder may now be supplied by all three pressure lines. The hydraulic control system hence becomes that shown in Fig. 12. The control system is now appended by a pressure line selector (PLS) and a switching scheme. The PLS online identifies which pressure lines that should be active for a given cylinder. The identified active pressure lines are thereafter forwarded in the switching vector, \mathcal{S} , to the switching scheme. The switching scheme divides the controller output, being the flow references Q_p^* and Q_r^* , between the six valves based on the switching vector \mathcal{S} .

5.1 Pressure Line Selector

Based on experience obtained through developing the PLS, the following requirements have been set up:

- The active pressure line(s) on the piston side should always be able to deliver the flow reference Q_p^* .
- The active pressure line(s) on the rod side should always be able to deliver the flow reference Q_r^* .
- The active piston and rod side pressure lines should yield the lowest possible throttling losses across the valves.

The developed solution identifies two active pressure lines for both the rod and piston side simultaneously. One of the identified pressure lines should be able to deliver the flow reference if it is positive and the other if it is negative. Additionally, it is developed such that the identified pressure lines result in the lowest throttling loss of those fulfilling the above requirement. The pressure line yielding the lowest loss is that with a pressure closest to the cylinder pressure. However, a certain pressure difference across the valve is necessary to deliver a flow through the valve, e.g. 5 bar for nominal flow. The active pressure line should hence be a margin above the cylinder pressure for a positive flow reference and below for a negative flow reference. The active pressure lines are hence identified by

$$\begin{aligned}
 p_{p,\text{supply}} &= \min(\{x \in \mathbf{p}_{\text{line}} \mid x \geq p_p + p_{\text{marg}}\}) \\
 p_{p,\text{return}} &= \max(\{x \in \mathbf{p}_{\text{line}} \mid x \leq p_p - p_{\text{marg}}\}) \\
 p_{r,\text{supply}} &= \min(\{x \in \mathbf{p}_{\text{line}} \mid x \geq p_r + p_{\text{marg}}\}) \\
 p_{r,\text{return}} &= \max(\{x \in \mathbf{p}_{\text{line}} \mid x \leq p_r - p_{\text{marg}}\})
 \end{aligned} \quad (32)$$

$\mathbf{p}_{\text{line}} = [p_{\text{HP}} \ p_{\text{IP}} \ p_{\text{LP}}]$ is a vector containing the pressures in the three pressure lines and $p_{\text{marg}} = 5$ bar is the pressure margin. As an example, the first expression in (32) is used to determine the active pressure line on the piston side for a positive flow reference, where the pressure line is used to supply flow to the cylinder. Initially, those pressure lines being able to deliver a positive flow are identified by the inequality condition $\mathbf{p}_{\text{line}} \geq p_p + p_{\text{p-marg}}$. Subsequently, the optimal pressure line is identified as that having the minimum pressure of those fulfilling the inequality condition. Considering the cylinder chamber pressure to always be between the pressure in the high and low pressure line, some observations may be made.

- The supply line is always either the high or intermediate pressure line.
- The return line is always either the intermediate or low pressure line.

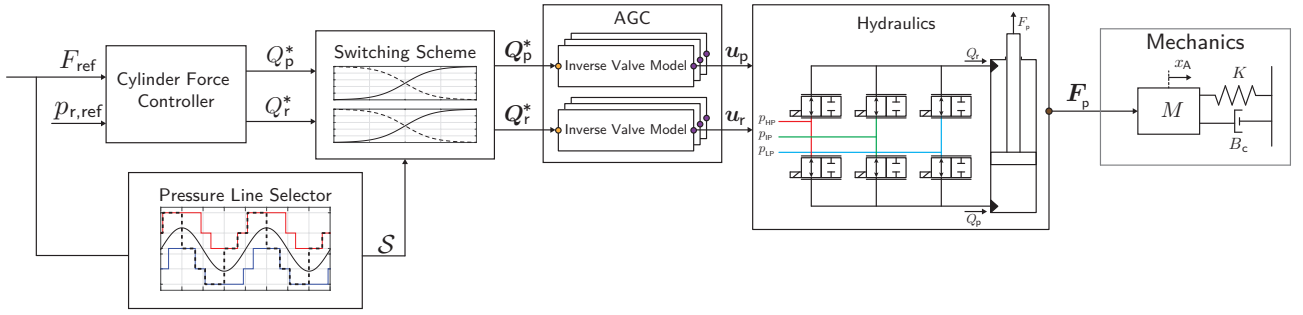


Figure 12: Structure of the complete hydraulic control system of the MPL concept.

As a result, it is not possible to utilize all force states shown in Fig. 2 if the requirement to the flow direction has to be satisfied. To avoid rapidly switching back and forth between active pressure lines, a minimum time of 500 ms between each switch has been implemented. With the active pressure lines determined, the available force, F_{avail} , may be calculated based on the direction of the flow references, given by

$$F_{\text{avail}} = \begin{cases} A_p p_{p,\text{supply}} - A_r p_{r,\text{return}} & \text{if } Q_p^* \geq 0 \wedge Q_r^* < 0 \\ A_p p_{p,\text{return}} - A_r p_{r,\text{supply}} & \text{if } Q_p^* < 0 \wedge Q_r^* \geq 0 \\ A_p p_{p,\text{supply}} - A_r p_{r,\text{supply}} & \text{if } Q_p^* \geq 0 \wedge Q_r^* \geq 0 \\ A_p p_{p,\text{return}} - A_r p_{r,\text{return}} & \text{if } Q_p^* < 0 \wedge Q_r^* < 0 \end{cases} \quad (33)$$

The last two cases of (33) only exist transiently, where the active pressure line on both the piston and rod side is either supplying or receiving flow. It is worth noting that the utilized pressure line combination is solely determined by the cylinder chamber pressures. Since the cylinder chamber pressures are products of the force and the rod side pressure reference with the used strategy, the rod side pressure reference solely determines the active pressure lines.

The output of the pressure line selector is the switching vector \mathcal{S} . With the proposed strategy there is always identified two pressure lines on both the rod and piston side, one which may deliver flow and one which may receive flow. An active pressure line has a switching vector value of 1 and an inactive has a value of 0. As an example, the identified supply and return lines may look like those in (34), which yields the switching vector \mathcal{S} in (35).

$$p_{p,\text{supply}} = p_{\text{HP}} \quad p_{p,\text{return}} = p_{\text{IP}} \quad p_{r,\text{supply}} = p_{\text{IP}} \quad p_{r,\text{return}} = p_{\text{LP}} \quad (34)$$

$$\mathcal{S} = \left[\underbrace{\text{HP IP LP}}_{\text{piston}} \quad \underbrace{\text{HP IP LP}}_{\text{rod}} \right]^T = \left[1 \ 1 \ 0 \ 0 \ 1 \ 1 \right]^T \quad (35)$$

The identified switching vector is afterwards given as input to the switching scheme.

5.2 Switching Scheme

The switching scheme is used to divide the flow references between the active pressure lines, while minimizing pressure oscillations when switching between pressure lines. The switching scheme has the structure shown in Fig. 13.

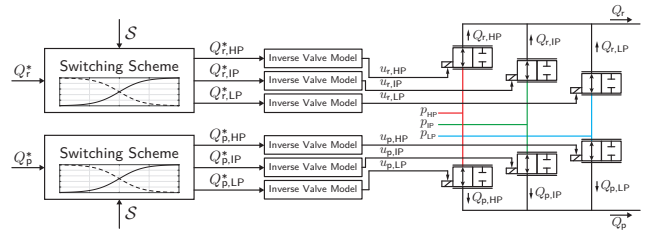


Figure 13: Structure used to divide the flow references.

It may be seen that the switching scheme divides the flow reference Q_p^* and Q_r^* among the three valves on the piston and rod side respectively based on the switching vector \mathcal{S} . This way each valve has a flow reference which is ideally delivered physically if the inverse valve model is consistent with the physical valve.

A switch is initiated every time one of the values in the switching vector \mathcal{S} is changed. The switching of the supply and return line is handled individually on both the rod and piston side. For simplicity, the following section is written for the piston side. As an example, the values in the switching vector are changed as

$$\mathcal{S} = \left[0 \ 1 \ 1 \ 0 \ 1 \ 1 \right]^T \longrightarrow \mathcal{S} = \left[1 \ 0 \ 1 \ 0 \ 1 \ 1 \right]^T \quad (36)$$

When the switch is initiated, the switching time for the piston side supply pressure is saved, $t_{p,\text{supply}}$. Additionally, since the switch takes numerous samples, the previous active pressure line is saved, $p_{p,\text{supply-prev}}$. These variables are used to generate functions for dividing the flow references among the valves. The same approach is used to determine the variables $t_{p,\text{return}}$ and $p_{p,\text{return-prev}}$ for the piston side return line. Several

switching function shapes have been tested, where a hyperbolic tangent function yields the best result with respect to pressure pulsations. The piston side switching functions for the supply and return lines are given by (37) and (38) respectively.

$$\Psi_{p,\text{supply}}(t) = \frac{1}{2} (1 + \tanh(\gamma_s (t - t_{p,\text{supply}} - T_s)))$$

$$\Psi_{p,\text{supply-prev}}(t) = 1 - \Psi_{p,\text{supply}}(t) \quad (37)$$

$$\Psi_{p,\text{return}}(t) = \frac{1}{2} (1 + \tanh(\gamma_s (t - t_{p,\text{return}} - T_s)))$$

$$\Psi_{p,\text{return-prev}}(t) = 1 - \Psi_{p,\text{return}}(t) \quad (38)$$

$\Psi_{p,\text{supply}}$ and $\Psi_{p,\text{supply-prev}}$ are the switching function for the current and previously active supply lines on the piston side. Similarly, $\Psi_{p,\text{return}}$ and $\Psi_{p,\text{return-prev}}$ are switching functions for the current and previously return lines. T_s and γ_s are constants which specify the switching time period and the slope of the switching functions respectively. The utilized switching functions given by (37) have the shapes shown in Fig. 14.

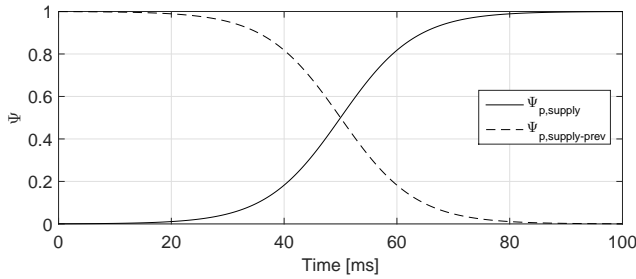


Figure 14: Hyperbolic tangent switching functions used for switching between pressure lines.

The switching is initiated at time 0 and takes approximately 100 ms from the switching is initiated until it has finished, when using $T_s = 50$ ms and $\gamma = 75$. Several combinations of these constants have been tested, where those used for illustration in Fig. 14 are chosen, since an increase in the switching time did not reduce the pressure pulsations any further.

Based on the switching functions $\Psi_{p,\text{supply}}$, $\Psi_{p,\text{supply-prev}}$, $\Psi_{p,\text{return}}$ and $\Psi_{p,\text{return-prev}}$, as well as the identified pressure lines $p_{p,\text{supply}}$, $p_{p,\text{supply-prev}}$, $p_{p,\text{return}}$ and $p_{p,\text{return-prev}}$, flow division functions may be created. The flow division functions are determined by (39), (40) and (41) for the HP, IP and LP line on the piston side respectively.

$$\Psi_{p,\text{HP}} = \begin{cases} \Psi_{p,\text{supply}} & \text{if } p_{p,\text{supply}} = p_{\text{HP}} \\ 0 & \text{otherwise} \end{cases} + \begin{cases} \Psi_{p,\text{supply-prev}} & \text{if } p_{p,\text{supply-prev}} = p_{\text{HP}} \\ 0 & \text{otherwise} \end{cases} \quad (39)$$

$$\Psi_{p,\text{IP}} = \underbrace{\begin{cases} \Psi_{p,\text{supply}} & \text{if } p_{p,\text{supply}} = p_{\text{IP}} \\ 0 & \text{otherwise} \end{cases}}_{\Psi_{p,\text{IP-supply}}} + \underbrace{\begin{cases} \Psi_{p,\text{supply-prev}} & \text{if } p_{p,\text{supply-prev}} = p_{\text{IP}} \\ 0 & \text{otherwise} \end{cases}}_{\Psi_{p,\text{IP-return}}} \quad (40)$$

$$\Psi_{p,\text{LP}} = \begin{cases} \Psi_{p,\text{return}} & \text{if } p_{p,\text{return}} = p_{\text{LP}} \\ 0 & \text{otherwise} \end{cases} + \begin{cases} \Psi_{p,\text{return-prev}} & \text{if } p_{p,\text{return-prev}} = p_{\text{LP}} \\ 0 & \text{otherwise} \end{cases} \quad (41)$$

The flow division functions always have a value between zero and one. Additionally, the sum of $\Psi_{p,\text{HP-supply}} + \Psi_{p,\text{IP-supply}} = 1$ and $\Psi_{p,\text{IP-return}} + \Psi_{p,\text{LP-return}} = 1$ at any time. The same approach as that described for the piston side may be used to determine the rod side flow division functions.

6 Pressure Reference Shaping

The rod side pressure reference is generated online by only knowing the current force reference, as well as the high and low pressure set-points. For a sinusoidal force reference, it is shaped such that it is in counter phase with the force reference, i.e. when the force reference is high, the rod side pressure reference is low and vice versa. A linear relationship is used and is given as

$$p_{r,\text{ref}} = a_{\text{ref}} F_{\text{ref}} + b_{\text{ref}} \quad (42)$$

$$a_{\text{ref}} = \frac{p_{\text{HP,set}} - p_{\text{LP,set}}}{F_{\text{min}} - F_{\text{max}}} \quad b_{\text{ref}} = p_{\text{HP,set}} - a_{\text{ref}} F_{\text{min}}$$

F_{max} and F_{min} are the maximum and minimum available forces. The maximum and minimum available forces are determined by

$$\begin{aligned} F_{\text{max}} &= A_p p_{\text{HP,set}} - A_R p_{\text{LP,set}} \\ F_{\text{min}} &= A_p p_{\text{LP,set}} - A_R p_{\text{HP,set}} \end{aligned} \quad (43)$$

where $p_{\text{HP,set}} = 350$ bar and $p_{\text{LP,set}} = 20$ bar are the pressure reference to the high and low pressure line respectively. With this shaping method it has been found that the intermediate pressure line tends to be self balancing, why an approximately constant pressure is obtained at the midpoint between the high and low pressure. The reason for this balancing is that the force states are selected based on the intermediate pressure level. If the intermediate pressure is high, the selected force states tend to drain the pressure line, while the selected force states tend to fill the pressure line if the intermediate pressure is low.

It is identified that an improved pressure reference may be constructed that lowers the throttling loss further if the force reference is pre-known. However, the

relative decrease in energy consumption is identified to be less than 10 %. Additionally, the balancing of the intermediate pressure line has to be taken care of actively with more sophisticated pressure references.

7 Performance Evaluation

The performance evaluation is based on simulation results obtained by use of the complete non-linear model with the developed hydraulic control system implemented. The objective of the performance evaluation is to determine the feasibility of the MPL concept, by comparing the obtained theoretical results to those obtained with the conventional separate metering concept shown in Fig. 11. The pressures in the pressure lines are shown in Fig. 15 for the 6 cylinders with the previously presented cyclic loads.

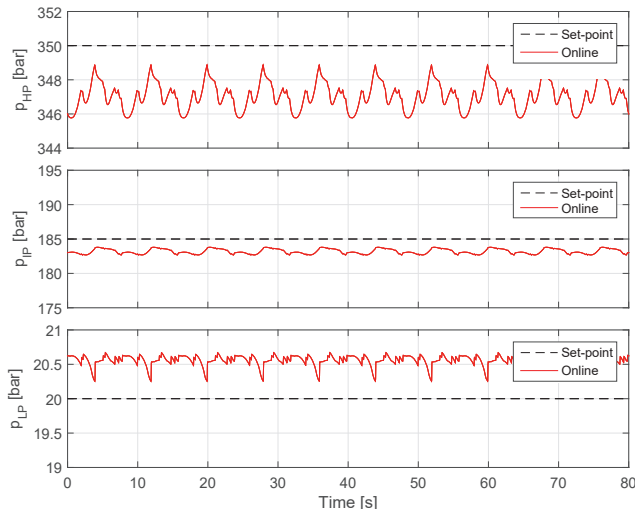


Figure 15: Pressure levels of the three pressure lines with the online pressure reference shaping method.

It is seen that the high and low pressure line have a slight steady-state offset due to the use of a simple proportional controller. The intermediate pressure is however seen to be very smooth and self-balancing close to the mid-point pressure between the high and low pressure with the online pressure reference shaping method.

The obtained force control performance when using the MPL concept is shown in Fig. 16.

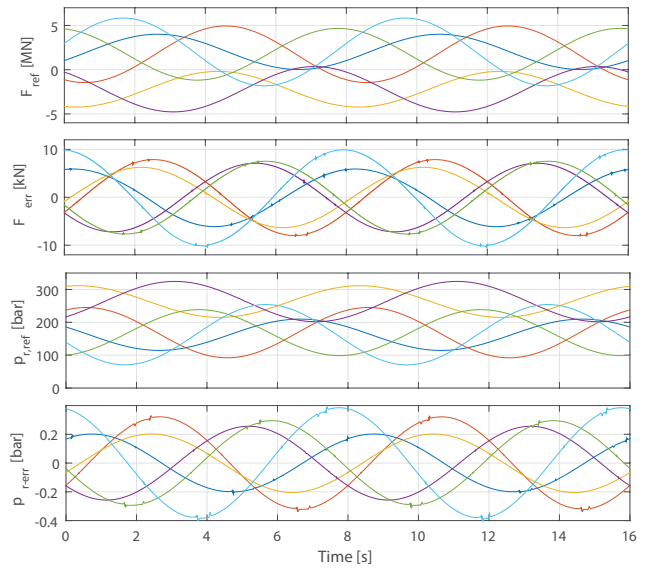


Figure 16: Simulated system response for cylinder force control using three pressure lines.

The force trajectory tracking obtained when switching between the three pressure lines is similar to that obtained when using two pressure lines in Fig. 11. The maximum force error is seen to be ± 10 kN, which is the same when using two pressure lines. Since similar control performance has been obtained when using three pressure lines, the developed switching system is validated. If looking carefully it is seen that there are a higher number of fluctuations (pressure ripples) when using three pressure lines due to switchings. It should however be noticed that the spikes have a magnitude less than 0.02 bar and should therefore be of no concern.

To evaluate on the switching performance several internal variables are shown in Fig. 17 for the light blue load case in Fig. 16. It is seen that the chosen force states are not always the optimal ones yielding the lowest losses, but they are a clear improvement compared to a conventional system. The rod side pressure is seen to be in counter-phase with the force reference and a further reduction in throttling losses would require a much more sophisticated shaping of the rod side pressure. The flows are seen to be very smooth even when a switch occurs or the direction of movement is changed.

7.1 Energy consumption

As mentioned earlier, the shaping of the rod side pressure reference is made with the objective of minimizing the area between the available force and obtained force. Using this method the cylinder velocity influence on the throttled power is neglected. An investigation of the throttled power, P_{throttle} , which is determined by (44),

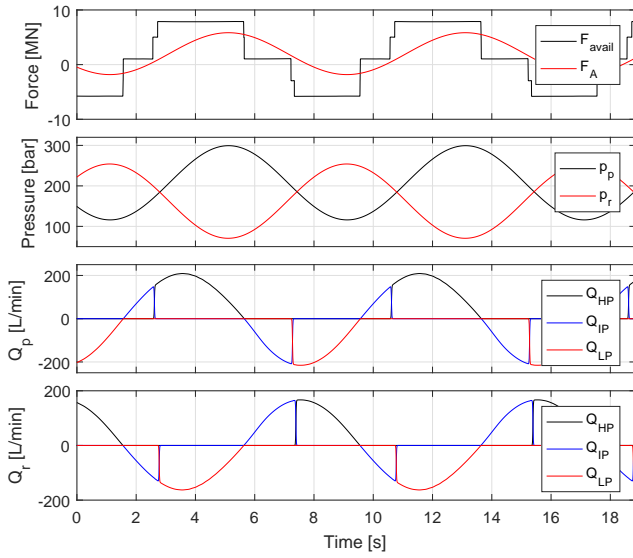


Figure 17: Simulation result of internal model variables of the MPL system.

has been made.

$$P_{\text{throttle}} = |(F_{\text{avail}} - F_p) \dot{x}_A| \quad (44)$$

The simulation results for comparison of the throttled power using the online pressure reference shaping method for the MPL concept, as well as that of a conventional hydraulic system are shown in Fig. 18 for the six load cases. As evident, the mean throttled power has been significantly reduced by the MPL concept compared to that of the conventional. To evaluate on the feasibility of the MPL concept a comparison of the energy consumptions is made. For both the MPL and the conventional system, the hydraulic supply energy may be determined based on the pump flow and the pressure in the high pressure line. The hydraulic energy consumption is calculated by (45).

$$E_{\text{in}} = \int_0^T Q_{\text{pump}}(t) p_{\text{HP}}(t) dt \quad (45)$$

Where T is the time that it takes to go through a relative high number of cycles (> 30). With the six used test cycles, the energy consumption has been averagely reduced by 49.3% when compared to the conventional concept. However, the energy reduction is highly dependent on the load case. As mentioned earlier, a further energy reduction may be obtained if a more optimal pressure reference is used, which would however require pre-known information about the force reference. Optimal shaping of the pressure reference for the given test cases has yielded up to 60% energy consumption reduction.

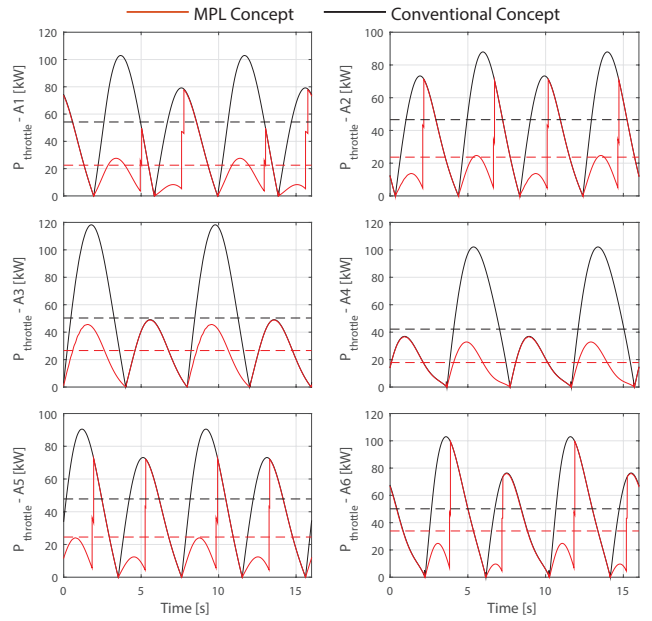


Figure 18: Throttled power comparison between MPL concept using online pressure reference shaping, as well as for a conventional system.

Conclusion

It has been proven that the theoretical control performance of the Multiple Pressure Line (MPL) concept is adequately similar to that of a conventional fluid power system, such that the performance may be regarded as identical. The obtained control performance using an online pressure reference shaping method is considered advantageous since no pre-knowledge about the cylinder force reference is required while yielding only a minor increase in energy consumption compared to a optimal shaped reference. An average energy consumption reduction of 49.3% has been obtained for six cylinders with different load cases, which indicates that the proposed concept and control structure has a great potential. With the proposed control structure, switching system and online shaping method, a simple solution has been developed. It is therefore assessed that the proposed solution is ready for experimental validation on a hydraulic cylinder drive with three pressure lines.

Appendix

Name	Description	Value	Unit
Hydraulics			
A_p	Piston side area	0.238	m ²
A_r	Rod side area	0.180	m ²
$V_{p,init}$	Initial piston side volume	0.0438	m ³
$V_{r,init}$	Initial rod side volume	0.0651	m ³
V_{line}	Oil volume of the three pressure lines	[0.123 0.062 0.062]	m ³
ω_v	Parker NG25 eigen-frequency	95	Hz
ζ_v	Parker NG25 damping coefficient	0.7	-
τ_v	Parker NG25 slew rate (normalized)	95	m/s
Q_n	Parker NG25 nominal flow	380	L/min
Δp_n	Parker NG25 nominal pressure drop	5	bar
ω_p	Pump eigen-frequency	10	Hz
ζ_p	Pump damping coefficient	1	-
τ_p	Pump slew rate	5	1/s
K_{pump}	Pump flow gain	250	L/min
D_s	Supply line diameter	50.8	mm
l_s	Supply line length	30	m
Cylinder friction constants			
F_c	Constant Coulomb friction	52.27	kN
k_{Cp}	Pressure dependent Coulomb friction	0.0048	m ²
B_c	Viscous friction	1.05	MNs/m
aBr	Stribeck to Coulomb factor	1	-
v_{br}	Break-away velocity	0.01	m/s
Simple pressure line constants			
V_{acc}	Accumulator volume	[0.3 0.3 0.05]	m ³
p_{g0}	Pre-charge gas pressure	[310.5 157.5 13.5]	bar
κ	Adiabatic gas constant	1.4	-
p_{line}	Pressure setpoint for the three lines	[350 - 20]	bar

Table 1: Model constants.

References

- Dengler, P. and von Dombrowski, R. Efficiency optimization of a hydrostatic system using an intermediate pressure line. *The 7th FPNI PhD Symposium on Fluid Power*, 2012.
- Dengler, P., Geimer, M., Baum, H., Schuster, G., and Wessing, C. Efficiency improvement of a constant pressure system using an intermediate pressure line. *8th International Fluid Power Conference*, 2012.
- Dengler, P., Groh, J., and Geimer, M. Valve control concepts in a constant pressure system with an intermediate pressure line. *21st International Conference on Hydraulics and Pneumatics, Ostrava, Czech Republic*, 2011.
- Ehsan, M., Rampen, W. S., and Salter, S. H. Modeling of digital-displacement pump-motors and their application as hydraulic drives for nonuniform loads. *Journal of Dynamic Systems, Measurement, and Control*, Vol. 122, 1997. doi:10.1115/1.482444.
- Guanzhong, Y. and Jihai, J. Power characteristics of a variable hydraulic transformer. *Chinese Journal of Aeronautics*, Vol 28, Iss. 3, 2015. doi:10.1016/j.cja.2015.04.008.
- Hansen, R. H., Kramer, M. M., and Vidal, E. Discrete displacement hydraulic power take-off system for the wavestar wave energy converter. *Energies*, 6, 4001-404, 2013. doi:10.3390/en6084001.
- Heikkila, M. and Linjama, M. Displacement control of a mobile crane using a digital hydraulic power management system. *Mechatronics*, 23(4), 452461, 2013. doi:10.1016/j.mechatronics.2013.03.009.
- Heikkila, M., Tammisto, J., Huova, M., Huhtala, K., and Linjama, M. Experimental evaluation of a piston-type digital pump-motor-transformer with two independent outlets. *ASME/Bath Symposium on Fluid Power and Motion Control, FPMC, Bath, UK*, 2010.
- Heybroek, K., Larsson, J., and Palmberg, J.-O. Open circuit solution for pump controlled actuators. *Proceedings of the 4th FPNI-PhD symposium. Sarasota, US*, 2006.
- Heybroek, K., Palmberg, J.-O., Lillemets, J., Lugnberg, M., and Ousbck, M. Evaluating a pump controlled open circuit solution. *Proceedings of the 51th International Exposition for Power Transmission, Nevada, USA*, 2008.
- Inderelst, M., Sgro, S., and Murrenhoff, H. Energy recuperation in working hydraulics of excavators. *Fluid Power and Motion Control Symposium, FPMC*, 2010.
- Ivantysynova, M. and Rahmfeld, R. Energy saving hydraulic actuators for mobile machinery. *1st Bratislavian fluid power symposium*, 1998.
- Ketelsen, S., Schmidt, L., Donkov, V. H., and Andersen, T. O. Energy saving potential in knuckle boom cranes using a novel pump controlled cylinder drive. *Modeling, Identification and Control, Vol. 39, pp. 73-89*, 2018. doi:10.4173/mic.2018.2.3.
- Linjama, M. and Huhtala, K. Digital hydraulic power management system - towards lossless hydraulics. *The third workshop of digital fluid power, Tampere Finland*, 2010.
- Mingdong, C. and Dingxuan, Z. Research on boom energy recovery system with closed circuit in hydraulic excavators. *Proc. of the International Conference on Transportation, Mechanical, and Electrical Engineering (TMEE)*, 2011. doi:10.1109/TMEE.2011.6199361.
- Parker. Characteristics 2 way high-response valve series tdp. 2015. URL http://www.parker.com/literature/Hydraulic%20Controls%20Europe/HY11-3500UK/PDF_2013/TDP%20UK.pdf. Accessed 8-11-2018.

Payne, G. S., Stein, U. P. P., Ehsan, M., Caldwell, N. J., and Rampen, W. H. S. Potential of digital displacement hydraulics for wave energy conversion. *In Proc. of the 6th European Wave and Tidal Energy Conference, Glasgow UK.*, 2005.

Schmidt, L., Groenkjaer, M., Pedersen, H. C., and Andersen, T. O. Position control of an over-actuated direct hydraulic cylinder drive. *Control Engineering Practice* 64, 1-14, 2017. doi:[10.1016/j.conengprac.2017.04.003](https://doi.org/10.1016/j.conengprac.2017.04.003).

Schmidt, L., Roemer, D. B., Pedersen, H. C., and Andersen, T. O. Speed-variable switched differential pump system for a direct operation of hydraulic cylinders. *Proc. of ASME/Bath Symposium on Fluid Power & Motion Control, Chicago, Illinois USA*, 2015. doi:[10.1115/FPMC2015-9575](https://doi.org/10.1115/FPMC2015-9575).

Shen, W., Jiang, J., Su, X., and Karimi, H. R. Energy-saving analysis of hydraulic hybrid excavator based on common pressure rail. *The Scientific World Journal*, 2013. doi:[10.1155/2013/560694](https://doi.org/10.1155/2013/560694).

Zimmerman, J. and Ivantysynova, M. Hybrid displacement controlled multi-actuator hydraulic systems. *The Twelfth Scandinavian International Conference on Fluid Power, Tampere, Finland*, 2011.